AGU PUBLICATIONS

JGR

Journal of Geophysical Research: Oceans

RESEARCH ARTICLE

10.1002/2016JC011826

Impact of current speed on mass flux to a model flexible seagrass blade

Jiarui Lei[1] and Heidi Nepf[1]

[1]Department of Civil and Environmental Engineering, Massachusetts Institute of Technology, Cambridge, Massachusetts, USA

Key Points:
- Flow over sufficiently pronated, smooth blades resembles flow over a flat plate, on which a laminar boundary layer may develop
- For pronated blades, the laminar boundary layer model correctly predicted the measured transfer velocity, with $K \propto U^{0.5}$
- Mass exchange at the blade scale controls the uptake at the meadow scale

Supporting Information:
- Table S1

Correspondence to:
J. Lei,
garylei@mit.edu

Citation:
Lei, J., and H. Nepf (2016), Impact of current speed on mass flux to a model flexible seagrass blade, *J. Geophys. Res. Oceans*, *121*, 4763–4776, doi:10.1002/2016JC011826.

Received 23 MAR 2016
Accepted 9 JUN 2016
Accepted article online 10 JUN 2016
Published online 10 JUL 2016

Abstract Seagrass and other freshwater macrophytes can acquire nutrients from surrounding water through their blades. This flux may depend on the current speed (U), which can influence both the posture of flexible blades (reconfiguration) and the thickness of the flux-limiting diffusive layer. The impact of current speed (U) on mass flux to flexible blades of model seagrass was studied through a combination of laboratory flume experiments, numerical modeling and theory. Model seagrass blades were constructed from low-density polyethylene (LDPE), and 1, 2-dichlorobenzene was used as a tracer chemical. The tracer mass accumulation in the blades was measured at different unidirectional current speeds. A numerical model was used to estimate the transfer velocity (K) by fitting the measured mass uptake to a one-dimensional diffusion model. The measured transfer velocity was compared to predictions based on laminar and turbulent boundary layers developing over a flat plate parallel to flow, for which $K \propto U^{0.5}$ and $\propto U$, respectively. The degree of blade reconfiguration depended on the dimensionless Cauchy number, Ca, which is a function of both the blade stiffness and flow velocity. For large Ca, the majority of the blade was parallel to the flow, and the measured transfer velocity agreed with laminar boundary layer theory, $K \propto U^{0.5}$. For small Ca, the model blades remained upright, and the flux to the blade was diminished relative to the flat-plate model. A meadow-scale analysis suggests that the mass exchange at the blade scale may control the uptake at the meadow scale.

1. Introduction

Seagrass provides a variety of ecosystem services. It supports biodiversity by providing habitat and shelter areas for various fisheries [*Costanza et al*., 1997] and by supplying food for larger herbivorous animals such as the dugong and green turtle [*Waycott et al*., 2005]. Seagrass attenuates incoming waves and protects shorelines from erosion due to wave impact [e.g., *Koch et al*., 2009]. Submerged macrophytes can also benefit the surrounding ecosystem by retaining the nutrients within the local environment [*Barko and James*, 1998]. Acting as a carbon sink, seagrass sequesters a larger amount of carbon per hectare per year than rainforest [*Fourqurean et al*., 2012]. Because seagrass plays such an important role in its environment, its protection and restoration have become a major focus in coastal management [*Greiner et al*., 2013].

A better understanding of the optimal conditions for seagrass growth is important for seagrass restoration. In this paper we consider specifically how flow conditions impact potential nutrient uptake. Unlike terrestrial vegetation, seagrass can take up nutrients from leaf tissue in addition to root tissue [*Touchette and Burkholder*, 2000; *Romero et al*., 2006]. The proportion of nutrient uptake by leaves may directly affect the growth rate, since seagrass communities frequently occur in oligotrophic environments, which lack essential elements such as dissolved nitrogen and phosphorus [*Romero et al*., 2006]. Previous studies have shown that nutrient uptake rates increase with velocity, U, if the uptake is mass-transfer limited [*Bilger and Atkinson*, 1992; *Koch*, 1994; *Hurd et al*., 1996; *Thomas et al*., 2000]. However, above a certain velocity the rate of mass transported to the blade surface by diffusion may surpass the maximum rate at which seagrass can biologically incorporate the available nutrients. At this point, the uptake rate is biologically limited and not impacted by further increases in velocity. The transition between mass-transfer-limited and biologically-limited flux depends on biological factors such as enzyme activity and light availability, which affects the photosynthetic rate [*Koch*, 1994]. In this study, we focus on the mass-

© 2016. American Geophysical Union. All Rights Reserved.

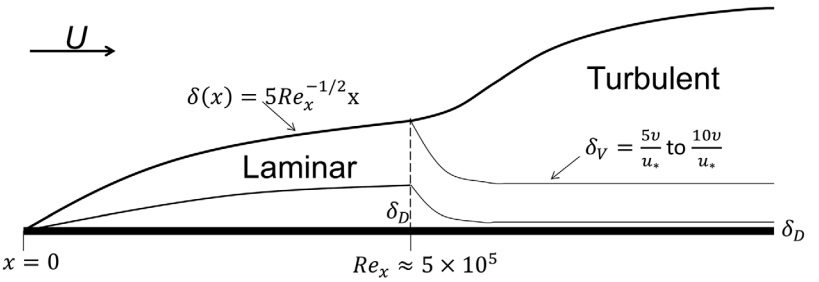

Figure 1. A laminar boundary layer (δ) evolves from the leading edge of a flat plate ($x = 0$), and becomes turbulent at the distance x corresponding to $Re_x = \frac{xU}{\nu} = 5\times10^5$. The viscous sublayer ($\delta_V$) remains laminar. The diffusive boundary layer, δ_D, is thinner than the viscous boundary layer, δ_V, with $\delta_D = \delta_V Sc^{-1/3}$ [*Kundu and Cohen*, 2002].

transfer limit, seeking to understand the relationship between flow velocity and potential flux of nutrients to seagrass blades under the mass-transfer limit. For simplicity and to isolate the physical transport processes, the experiments were conducted with individual model seagrass blades made of LDPE (low-density polyethylene) in unidirectional flows.

The mass flux per blade surface area (J (kg/m^{2}s)) may be described by a transfer velocity (K (m/s)),

$$J = K\Delta C \tag{1}$$

with ΔC (kg/m^3) the concentration difference between the bulk fluid and the blade surface. To derive a model for K we appeal to boundary layer theory. Assuming that a pronated seagrass blade approximates a flat plate (Figure 1), a viscous boundary layer grows with distance from the leading edge. Initially the boundary layer is laminar, even if the external flow is turbulent. As long as the boundary layer remains laminar, the boundary layer thickness, δ, can be described by the Blasius equation [e.g., *White*, 2008],

$$\delta(x) = 5Re_x^{-1/2}x, \quad Re_x = \frac{Ux}{\nu} \tag{2}$$

where x is the distance from the leading edge, U is the current speed, ν is the kinematic viscosity of water, and Re_x is the boundary layer Reynolds number. At some distance from the leading edge, defined by $Re_x = \frac{Ux}{\nu} \approx 5\times10^5$, the boundary layer becomes turbulent with a viscous sublayer. However, the presence of vigorous turbulence may cause an earlier transition [e.g., *Kosorygin* and *Polyakov*, 1990]. Once the boundary layer is turbulent, the viscous sublayer thickness is between

$$\delta_V = \frac{5\nu}{u_*} \text{ and } \frac{10\nu}{u_*} \tag{3}$$

with u_* the shear velocity [*Boudreau and Jorgensen*, 2001; *Kundu and Cohen*, 2002].

One limit of flux behavior can be defined if we assume that the transition to a turbulent boundary layer occurs at the leading edge, which might be reasonable if surface roughness on the blade is large enough to trip the boundary layer. In this case the viscous sublayer thickness is uniform along the blade. The diffusive boundary layer thickness δ_D, is related to the viscous boundary layer thickness δ_V through the Schmidt number Sc [*Boudreau and Jorgensen*, 2001]

$$\delta_D = \delta_V Sc^{-1/3}, \quad Sc = \frac{\nu}{D_W} \tag{4}$$

where D_W is the molecular diffusivity in water. A simple model for mass flux can then be constructed by assuming that outside the diffusive boundary layer the fluid is well-mixed by turbulence and the concentration of the solute in the water is uniform in the bulk fluid. Within the diffusive boundary layer, the concentration gradient is assumed to be linear between the bulk fluid concentration and the concentration at the blade surface. The mass flux across the diffusive boundary layer can then be described using Fick's law [*Stevens and Hurd*, 1997],

$$J = \frac{D_W}{\delta_D}\Delta C = K\Delta C, \quad K = \frac{D_W}{\delta_D} \tag{5}$$

where ΔC is now specifically the concentration difference across the diffusive boundary layer, and $K = \frac{D_W}{\delta_D}$ is the transfer velocity. For a given surface, u_* scales on U, so that equations (3), (4) and (5) indicate that the transfer velocity is linearly proportional to velocity, e.g., assuming $\delta_V = \frac{5\nu}{u_*}$,

$$K = \frac{D_W}{5\nu} u_* Sc^{1/3}, \quad K \propto U \tag{6}$$

Indeed, a linear relationship between transfer velocity and current speed has been observed for kelp blades [*Hurd et al*., 1996]. However, this relationship is not supported by field measurements with seagrass, for which the flux of nutrient to meadows under unidirectional current exhibit a dependence on velocity of $U^{0.4\pm0.2}$ [*Weitzman et al*., 2013; *Thomas et al*., 2000].

For an alternate model, we may assume that the blade is sufficiently smooth to maintain a laminar boundary layer over the length of the blade. Indeed, *Nishihara and Ackerman* [2009] observed a laminar boundary layer over the full length of individual leaves of a freshwater macrophyte. In addition, *Koch* [1994] showed that blades of the seagrass *Thalassia testudinum* with low epiphytic growth are hydrodynamically smooth over a wide range of current speeds, suggesting that a laminar boundary layer model is appropriate for these blades. Further, for a typical range of blade lengths, $L = 0.1$ to 0.6 m, the boundary layer will not become turbulent before the end of the blade (i.e., $Re_L < 10^5$) for current speeds up to 0.8 m/s. Assuming a laminar boundary layer is maintained over the entire blade length, the transfer velocity at distance x from the leading edge is $K(x) = 0.332x^{-1}D_w Re_x^{1/2} Sc^{1/3}$ [e.g., *Incropera and DeWitt*, 1996], from which the average transfer velocity along a blade of length L (denoted by overbar) is:

$$\bar{K} = \frac{1}{L}\int_0^L 0.332 D_W \sqrt{\frac{U}{\nu x}} Sc^{1/3} dx = 0.664 D_W \sqrt{\frac{U}{\nu L}} Sc^{1/3} \tag{7}$$

The laminar boundary layer model has been previously used to describe flux to individual leaves of terrestrial timber trees [e.g., *Grace et al*., 1980] and the freshwater macrophyte, *Vallisneria americana* [*Nishihara and Ackerman*, 2006].

In the flux models discussed above, the seagrass blade is modeled as a flat plate positioned parallel to the flow. However, depending on the current magnitude, the blade posture may vary from vertical (perpendicular to the flow) to strongly pronated (with most of the blade parallel to the flow). The change in plant posture in response to flow is known as reconfiguration, and the degree of reconfiguration is described by two dimensionless parameters, the Cauchy number *Ca*, which is the ratio of the hydrodynamic drag to the restoring force due to blade stiffness, and the Buoyancy parameter *B*, which is the ratio between restoring forces due to buoyancy and stiffness [*Luhar and Nepf*, 2011],

$$Ca = \frac{1}{2}\frac{\rho C_D b U^2 L^3}{EI}, \quad B = \frac{\Delta\rho g b h L^3}{EI} \tag{8}$$

where ρ is the density of water, C_D is the drag coefficient, b is the blade width, h is the blade thickness, $\Delta\rho$ is the difference in density between the water and the blade, E is the Young's modulus, and $I = \frac{bh^3}{12}$ is the second moment of inertia. Previous studies indicate that B is small for common seagrass species such as *Thalassia testudinum*, *Posidonia oceanica* and *Zostera marina* ($B \leq 1.4$, see Table 2), and, for this range of values, B does not play an important role in controlling blade posture [*Luhar and Nepf*, 2011]. For example, Figure 2 compares the reconfiguration predicted from the Luhar model for two blades ($B = 0$ and 10) across a range of *Ca*. If $Ca = 1$, the blade is nearly vertical in posture; if $Ca = 1000$, then 90% of the blade is pronated, resembling a flat plate parallel to flow. At these values of *Ca* (= 1 and 1000), the value of B (= 0 and 10) has little influence on the blade posture, and the curves for B = 0 and B = 10 overlap. For $Ca = 32$, there is a small influence from B, as the curve $B = 0$ is slightly more pronated than $B = 10$. Considering the range of postures shown in Figure 2, we expect that the flat plate model may apply for the pronated blades ($Ca \gg 1$), but not for upright blades ($Ca \leq 1$). In this study, we directly measure mass accumulation in model flexible blades at different values of *Ca* and use a numerical model to convert the measured mass accumulation to a transfer velocity. The dependence of transfer velocity (K) on current speed (U) is compared to the boundary layer models described by equations (6) and (7).

2. Materials and Methods

The model seagrass blades were constructed from low-density polyethylene (LDPE) film, which had a density of 0.925 g/cm^3 and a Young's modulus of 0.3 GPa [*Ghisalberti and Nepf*, 2002]. In order to cover a range of *Ca* experienced by real seagrass blades, three different blades were cut from 100 μm and 250 μm thick

Table 1. Model Blade Dimensions, *Ca* and *B* Values

Blade No.	Length (cm)	Thickness (um)	Velocity Range (cm/s)	Cauchy Number	Buoyancy Parameter
1	15	100	2.2–20.8	59–5300	13
2	10	100	2.2–20.8	17–1600	3.9
3	5	250	2.2–20.8	0.14–12	0.078

LDPE films (Table 1). All blades had a width of $b = 1$ cm. Using current speeds of $U = 2.2$ to 20.8 cm/s, we created experimental conditions with Ca from 0.14 to 5.3×10^3, which overlapped with a wide range of field conditions, as compared in Tables I and 2. The model blades had slightly higher values of Buoyancy parameter ($B = 0.08$ to 13) compared to real blades ($B = 10^{-5}$ to 1, Tables 1 and 2). However, as shown in Figure 2, over this range of B, the value of B does not significantly impact the blade posture, which is effectively controlled by the Cauchy number. As reported in *Folkard* [2005], the surface roughness of this plastic sheeting (coefficient of kinetic friction $\mu = 0.47 \pm 0.03$) is comparable to real seagrass without epiphytes ($\mu = 0.44 \pm 0.04$, *Posidonia oceanica*).

Laboratory experiments were carried out in a flume with a width of 38 cm and a length of 24 m. The flume was filled to 40 cm depth. Individual blades were inserted into the top of wooden cylinders mounted in a plastic board, which was placed on an acrylic ramp (12 cm high, 1 m long at top and 2 m long at bottom) positioned about 10m downstream from the flume inlet (Figure 3). Vertical profiles of stream-wise velocity were measured above the ramp with a 3D Nortek Vectrino Acoustic Doppler Velocimeter (ADV). Each measurement was made for a period of 2 min at a sampling rate of 200 Hz. The time-mean velocity was calculated as the average of all the samples. As shown in Figure 4, the velocity was vertically uniform starting 3 cm above the ramp surface. The blades were mounted on a cylindrical wooden post (length 8 cm; diameter 6mm), and in flow the blades extended vertically at most 23 cm above the ramp, so that the blades were positioned within the region of near-uniform velocity.

To measure the rate of mass flux to the model blades, we adapted the passive sampling method described in *Adams et al.* [2007], which uses LDPE to measure the concentration of organic chemicals in soil and water, taking advantage of the fact that hydrophobic organic compounds preferentially partition into LDPE. In the present experiments, the flume was dosed with 1, 2-dichlorobenzene and using the methods described below we determined the mass accumulated in the model blades after different exposure times, from which we inferred the transfer velocity, K, associated with different current speeds.

The partition coefficient, P_{PEW}, describes the ratio of 1, 2-dichlorobenzene concentration in the LDPE and in the water at equilibrium. We determined P_{PEW} from the following experiment. Six glass amber vials ($V_v = 40$ mL) were filled with milliQ water (18 MΩ) with an initial concentration of 1, 2-dichlorobenzene ($C_{w,i}$) of 40 ppb. To five of the vials we added 0.05 cm^3, 0.1 cm^3, 0.2 cm^3, 0.3 cm^3 and 0.5 cm^3 of LDPE (V_{PE}), respectively. The sixth vial was the control and did not contain LDPE. We assumed that the volume of the solution V_w was the same as the volume of the vial V_v, which was reasonable given that the volume of LDPE was two orders of magnitude smaller than the vial volume. The vials were put in the refrigerator for 7 days, after which 5 mL of the solution was withdrawn from each vial. The concentration of 1, 2-dichlorobenzene in the vial water (C_w) was measured using GC-FID (Gas chromatography with flame ionization detector) with an electron capture instrument (Perkin Elmer Autosystem XL) and a purge and trap system (Tekmar LSC 2000). The ratio between the initial concentration in the vial water, $C_{w,i}$, and the final concentration in the water, C_w, satisfies the following equation,

$$\frac{C_{w,i}}{C_w} = 1 + \frac{P_{PEW} V_{PE}}{V_w} \quad (9)$$

The partition coefficient $P_{PEW} = 380 \pm 40(SD)$ was determined based on the arithmetic mean and standard deviation (SD) of all P_{PEW} values calculated using

Table 2. Physical Parameters of Real Seagrass Blades

Physical Parameters	*Thalassi testudinum*[a]	*Zostera Marina*[b]	*Posidonia oceanica*[c]	Laboratory Experiments
Thickness, h(mm)	0.30–0.37	0.15–0.23	0.20	0.10, 0.25
Width, b(cm)	1	0.3 to 0.5	1	1
Length, L(m)	0.10–0.25	0.15–0.60	0.15–0.50	0.05, 0.10, 0.15
Density, ρ(kg/m^3)	940	700	910	920
Modulus, E(GPa)	0.4 to 2.4	0.26	0.47	0.3
B	0.00003–0.004	0.01–1.4	0.002–0.1	0.08–13
Ca	0.04–640	4–80,000	4–14,000	0.14–5300
Velocity, U(m/s)	0.02–0.2	0.02–0.2	0.02–0.2	0.02–0.2

[a] *Bradley and Houser* [2009].
[b] *Fonseca et al.* [2007] and *Abdelrhman* [2007].
[c] *Folkard* [2005].

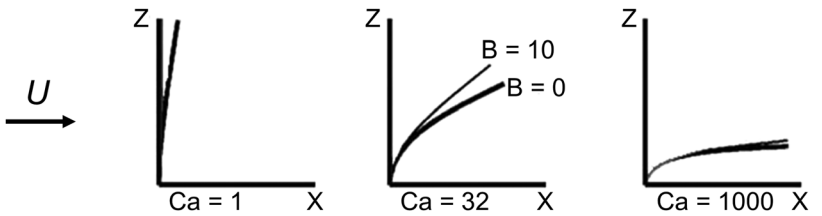

Figure 2. Blade posture predicted by *Luhar* model for different values of Cauchy number ($Ca = 1$, 32 and 1000) and two values of Buoyancy parameter ($B = 0$ and 10). In each subplot, $B = 0$ and 10 shown by thicker and thinner curves, respectively, as noted in the center subplot. For $Ca = 1$ and 1000, the two curves essentially overlap.

equation (9). After 14 days, we conducted the same GC measurements using 5 mL of the remaining solution in each vial. The concentration measurements done after 7 days and 14 days differed by an average of 5%, which demonstrated that 7 days was sufficient to reach equilibrium (Table 3).

Before beginning an experimental run in the water channel, we covered the whole channel with aluminum foil to reduce volatilization of the tracer chemical and to prevent dust from falling into the flume. At the start of a set of experiments, 250 μL of 1, 2-dichlorobenzene was injected into the flume over a time period equal to the recirculation time of the flume, so that the mixing over the flume volume could be accelerated. The channel was run at 20 cm/s for 30 minutes to ensure that the concentration was uniform throughout the flume, producing an initial concentration of 90 ppb. The time required to achieve a uniform concentration at 20 cm/s was determined by a tracer test with Rhodamine WT [*Rominger*, 2014, Appendix C]. After this the channel velocity was changed to one of the test velocities $U = 0$, 2.2 cm/s, 4.3 cm/s, 8.6 cm/s, 13.3 cm/s, and 20.8 cm/s. Six of the same blade as well as three back-up blades were placed in the channel (Figure 3c) and left in for 20 min, 60 min and 90 min. After each designated exposure time, two replicate blades were taken out of the flume, dried with kimwipes, and placed in individual clean 40 mL glass amber vials filled with milliQ water. Right after each blade was removed, an additional vial was filled with flume water to record the bulk fluid concentration (C_0). All blade and flume water samples were placed in the refrigerator for 9 days, which was sufficient to reach equilibrium (see the previous section and Table 3). The concentration of 1, 2-dichlorobenzene in the water of each equilibrated sample vial (C_w) was measured using GC-FID, and the associated concentration in the equilibrated blade was $C_w P_{PEW}$. From these equilibrated concentrations the original mass of 1, 2-dichlorobenzene in the blade when it was removed from the water channel can be calculated as $M_{PE} = C_w(V_w + P_{PEW}V_b)$, with V_w and V_b the volume of vial water and blade, respectively. The saturated uptake, $M_{sat} = C_0 P_{PEW} V_b$, is defined as the maximum mass of 1, 2-dichlorobenzene that the blade would take up from the flume water, if the exposure time was unlimited. The ratio of measured mass uptake (M_{PE}) to the saturated mass uptake (M_{sat}) by the blade is

$$\frac{M_{PE}}{M_{sat}} = \frac{C_w(V_v + P_{PEW}V_b)}{C_0 P_{PEW} V_b} \tag{10}$$

The uncertainty in this ratio, $\Delta\frac{M_{PE}}{M_{sat}}$, was calculated by propagating the uncertainty in C_w, C_0, V_v, V_b, and P_{PEW}, following *Taylor* [1997]. The largest uncertainty was contributed by C_w, which

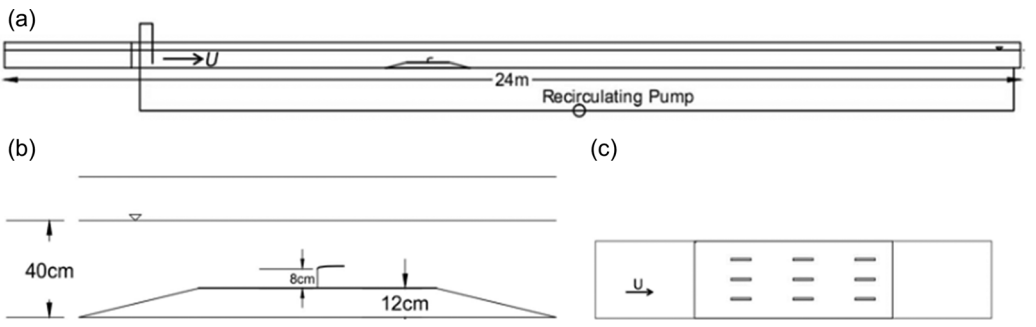

Figure 3. Experiment setup (a) side view of entire flume; (b) close-up side view of the ramp with a single blade on post; (c) top-view of the ramp showing the positions of blades at the start of a flux measurement experiment. Individual blades were removed from the flume after different durations of exposure.

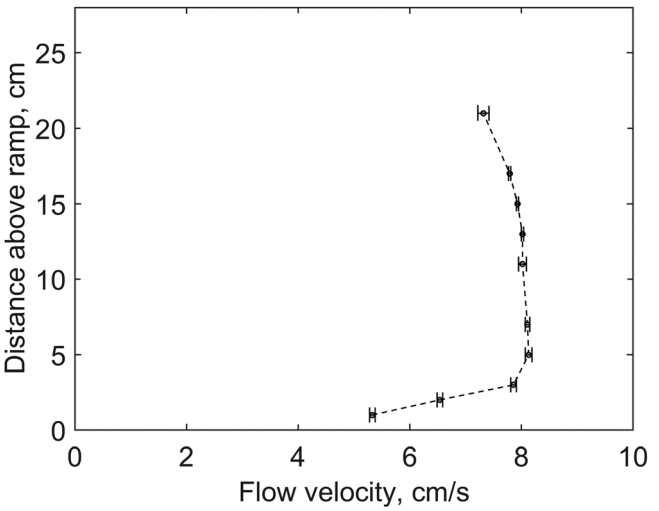

Figure 4. Velocity profile above the ramp surface. The horizontal error bars denote the 95% confidence interval on the mean.

reflected both the instrument uncertainty and the replicate uncertainty. The total uncertainty in C_w (15%) was larger than the replicate uncertainty (5%), so that two replicates was determined to be sufficient.

The transfer velocity, K, was determined by fitting the measured mass uptake to that predicted by a one-dimensional diffusion model in the direction z perpendicular to the blade surface (Figure 5). The concentration within the model blade (C_{PE}) evolved with time (t) following a one-dimensional diffusion equation

$$\frac{\partial C_{PE}}{\partial t} = D_{PE}\frac{\partial^2 C_{PE}}{\partial z^2} \tag{11}$$

with D_{PE} the diffusion coefficient within the LDPE blade. We neglected lateral and longitudinal diffusion because the blade width b and length L were much greater than the blade thickness, such that lateral and longitudinal diffusion timescales were long compared with the vertical (z) diffusion timescale. 1, 2-dichlorobenzene has molar volume $V_m = 113$, from which we used *Lohmann* [2012] to estimate $log\, D_{PE} = 0.0145V_m + 6.1$, which gives $D_{PE} = 1.8\times10^{-8}$ cm^2/s. We assumed that the flux to both sides of the blade was the same, so that from symmetry the concentration gradient at the blade centerline ($z = 0$) would be zero,

$$\left.\frac{\partial C_{PE}}{\partial z}\right|_{z=0} = 0 \tag{12}$$

Flow visualization was use to examine when flow symmetry (and thus flux symmetry) was a good assumption. The flux into the blade at the blade surface ($z = h/2$) was set equal to the flux delivered to the blade (J), as described by equation (1).

$$D_{PE}\left.\frac{\partial C_{PE}}{\partial z}\right|_{z=h/2} = J = \Delta CK = \left(C_0 - \frac{C_{PE}|_{z=h/2}}{P_{PEW}}\right)K \tag{13}$$

Equations (11)–(13) were solved using finite difference to find $C_{PE}(z)$ between the blade centerline, $z = 0$, and the top surface $z = h/2$. The vertical grid size was 1.0 μm and 2.5 μm for the 100 μm and 250 μm thick blades, respectively. The time step was reduced until the solution converged (became independent of the time step), which occurred for a time step of 0.01 seconds. After finding $C_{PE}(z)$ numerically, $\frac{M_{PE}}{M_{sat}}$ was calculated as

$$\frac{M_{PE}}{M_{sat}} = \frac{2bL\int_0^{h/2} C_{PE}(z)dz}{2bLC_0} = \frac{1}{C_0}\int_0^{h/2} C_{PE}(z)dz \tag{14}$$

Table 3. Data for Determining P_{PEW}

Vial No.	V_{PE}	$\frac{V_{PE}}{V_w}$	$\frac{C_{w,i}}{C_w}$ (7 days)	$\frac{C_{w,i}}{C_w}$ (14 days)	Relative Difference[a]
1	No blade		1	1	
2	0.05 cm^3	$\frac{1}{800}$	1.2 ± 0.1	1.2 ± 0.1	1.7%
3	0.1 cm^3	$\frac{1}{400}$	2.1 ± 0.2	2.3 ± 0.2	9.5%
4	0.2 cm^3	$\frac{1}{200}$	3.0 ± 0.3	2.9 ± 0.3	1.0%
5	0.3 cm^3	$\frac{3}{400}$	3.4 ± 0.3	3.1 ± 0.3	6.8%
6	0.5 cm^3	$\frac{1}{80}$	5.4 ± 0.5	5.3 ± 0.5	2.6%

[a]The relative difference is defined as $100\%\times\left|\left(\frac{C_{w,i}}{C_w}\ (14\ \text{days}) - \frac{C_{w,i}}{C_w}(7\ \text{days})\right)\right| / \frac{C_{w,i}}{C_w}$ (7 days).

For each channel velocity, U, the mass uptake measurements provided values for $\frac{M_{PE}}{M_{sat}}$ and the uncertainty $\Delta\frac{M_{PE}}{M_{sat}}$ at $t = 20$ min, 60 min and 90 min. Using the numerical solution to equations (11)–(13), the lower bound of K was determined by fitting $\left(\frac{M_{PE}}{M_{sat}} - \Delta\frac{M_{PE}}{M_{sat}}\right)$, and the upper bound of K was determined by fitting $\left(\frac{M_{PE}}{M_{sat}} + \Delta\frac{M_{PE}}{M_{sat}}\right)$.

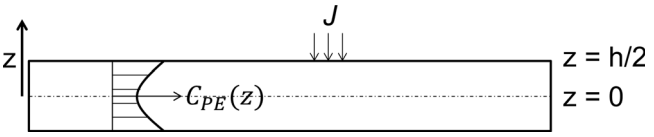

Figure 5. A schematic of the diffusion model. With the same flux (J) to both sides of the blade, the concentration distribution within the blade ($C_{PE}(z)$) is symmetric about the blade centerline, $z = 0$. Equations (11)–(13) were solved numerically between $z = 0$ and $z = h/2$.

Finally, the blade posture at each flow velocity was captured using a Canon Rebel T5i DSLR camera, which was mounted on a SIRUI tripod looking through the side of the flume. To better understand the flow near the blade boundary, a green fluorescent dye was injected close to the blade surface and excited by a UV light placed above the channel. Videos were taken using a Canon 5d Mark III DSLR camera. All the videos were analyzed using MATLAB image processing toolbox.

3. Results

As expected, the mass accumulated in the blades (M_{PE}) increased with increasing exposure time ($t = 20$, 60, 90 min), as shown in supporting information Table S1. The measured mass accumulation was fit to the mass accumulation model (equations (11)–(13)), using the transfer velocity (K) as the fitting parameter. In this way, a best-fit K was estimated for each experimental blade and flow condition. An example is shown in Figure 6 for Blade 1 (1 cm×15 cm×100 um) at 8.6 cm/s, for which the best-fit K was 5.5×10^{-6} m/s (with $K_{max}=7.6\times10^{-6}$ m/s and $K_{min}=3.9\times10^{-6}$ m/s).

For each blade, the transfer velocity increased with flow speed (Figure 7). For comparison, Figure 7 also includes the theoretical transfer velocity for a turbulent boundary layer (dashed lines, equation (6) using $\delta_V=\frac{5\nu}{u_*}$ and $\delta_V=\frac{10\nu}{u_*}$), and for a laminar boundary layer (solid line, equation (7)). The diffusivity of 1, 2 – dichlorobenzene in water is $D_W=0.79\times10^{-9}$ m^2/s [*NJDEP*,], and $\nu=1\times10^{-6}$ m^2/s. For the turbulent boundary layer model, we used the typical value $u_*=\frac{U}{10}$, which is consistent with a range of values suggested by measurements over other macrophytes. For example, measurements reported in *Nishihara and Ackerman* [2006] suggest that $u_* \approx \frac{U}{5}$ for the freshwater macrophyte *Vallisneria americana*. Similarly, from measurements reported in *Hansen et al*. [2011, Table 1], $u_* \approx 0.07U$ for the kelp *Macrocystis pyrifera*. For nearly all conditions the turbulent boundary layer model over-predicted the measured K, and it failed to capture the trend at the higher velocity range (Figure 7). For Blade 1 and Blade 2 (Figures 7a and 7b) the laminar boundary layer model agreed with the measured K within uncertainty over most of the velocity range. For Blade 3, both boundary layer models over-predicted the measured K.

The blade postures at a range of flow velocities (2.2 cm/s to 20.8 cm/s) for all three blades are shown in Figure 8. Blade 1 was associated with the highest Cauchy numbers (59–5300) and, consistent with this, exhibited the greatest pronation. Blade 2 was associated with a midrange of Ca (17–1600). Blade 3 was associated with the lowest Ca (0.14 to 12) and exhibited the least pronation. The observed pronation was consistent with that predicted by the Luhar model (Figure 9). Specifically, the deflected height predicted by equation 4 given in *Luhar and Nepf* [2013], was close to the observed deflected height.

In a separate experiment, dye (fluorescein) was injected at the top and bottom blade surfaces (Figure 10). For the highest Ca numbers (620 and 2200 in Figure 10), the blade was strongly pronated, and, dye injected on both the top and bottom surfaces flowed along the surface, indicating flow parallel to the blade surface, as assumed in the flat-plate boundary layer models (e.g., equation (7)). At lower Ca (=59, Figures 10e and 10f) the dye flowed along the top surface, but separated from the bottom surface. Finally, when the blade was close to vertical ($Ca = 0.53$, Figures 10g and 10h), dye injected on the front face quickly wrapped around the blade, similar to the flow pattern observed near a vertical bluff body. This flow pattern would not produce an evolving boundary layer along the blade length, as assumed in equation (7). To summarize, flow visualization suggested that a flux model based on a boundary layer developing over a flat plate would be appropriate at higher Ca, for which the blade is sufficiently pronated. In these cases, the assumption that the flux to both sides of the blade was the same (see equation (12)) would be reasonable, as both sides exhibit flow parallel to the blade over most of the blade length. However for lower Ca, the blade was only weakly pronated or close to vertical, and equation (7) would not be appropriate. The tracer study and blade postures suggest that this transition occurs at $Ca \approx 60$.

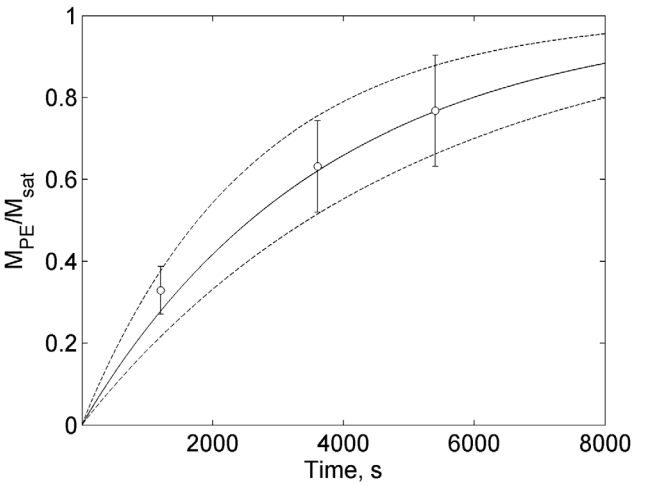

Figure 6. Symbols show the measured mass accumulation (M_{PE}) normalized by the saturated mass accumulation (M_{sat}) for Blade 1 (1 cm×15 cm×100 μm) at flow velocity U=8.6 cm/s. The best fit model prediction, with $K=5.5\times10^{-6}\,m/s$, is shown with solid line. The dashed curves indicate the fits corresponding to $K_{min}=3.9\times10^{-6}m/s$ (lower curve) and $K_{max}=7.6\times10^{-6}\,m/s$ (upper curve).

4. Discussion

Blade 1, which covered the highest range of *Ca* (= 59–5300), was strongly pronated over the entire velocity range, such that most of the blade length was parallel with the flow (Figure 8a). In addition, even at the highest velocity (U = 20.8 cm/s), the boundary layer along the entire blade length (L = 15 cm) was laminar based on the blade-scale Reynolds number, specifically $Re_L \approx 3\times10^4 < 5\times10^5$. Therefore, the flow along the blade matched the model assumption of a laminar boundary layer developing over a flat plate. Consistent with this, the measured transfer velocity agreed within uncertainty with the theoretical prediction provided by equation (7) (Figure 7a). In particular, the transfer velocity, K, followed the trend of $U^{0.5}$. The power-law fit of all data points was $K \propto U^{0.4\pm0.1}$. Blade 2, which covered the medium range of *Ca* (= 17–1600), was slightly less pronated than Blade 1 (Figure 8b). Nevertheless, except for the lowest flow velocity (U = 2.2 cm/s), most of the blade length was nearly parallel with the flow. The blade-scale Reynolds number at the highest velocity was $Re_L \approx 2\times10^4 < 5\times10^5$, such that the boundary layer remained laminar over the whole blade length. The transfer velocity measured for Blade 2 (*Ca* = 20–1700), also agreed with the theoretical model within uncertainty (Figure 7b), and the power-law fit $K \propto U^{0.4\pm0.1}$. In contrast, the transfer velocity measured for Blade 3 (*Ca* = 0.14 to 12) did not agree with the flat-plate laminar boundary layer theory (Figure 7c). At all current speeds, the flat-plate boundary layer model overestimated the transfer velocity. These observations suggested that the flat-plate boundary layer model was appropriate only when the blade was sufficiently pronated, corresponding to $Ca \geq 60$. At lower *Ca* the blade was close to vertical and water went around the blade rather than flowing along it. In this case, the flow near the blade did not approximate a boundary layer developed by flow parallel to a flat plate. More research is needed to characterize the flow near a nearly vertical inclined plate.

We also compared the measured transfer velocity to other theoretical models. First, the turbulent boundary layer model is included as a dashed line in Figures 7a–7c. This model did not agree with the measured

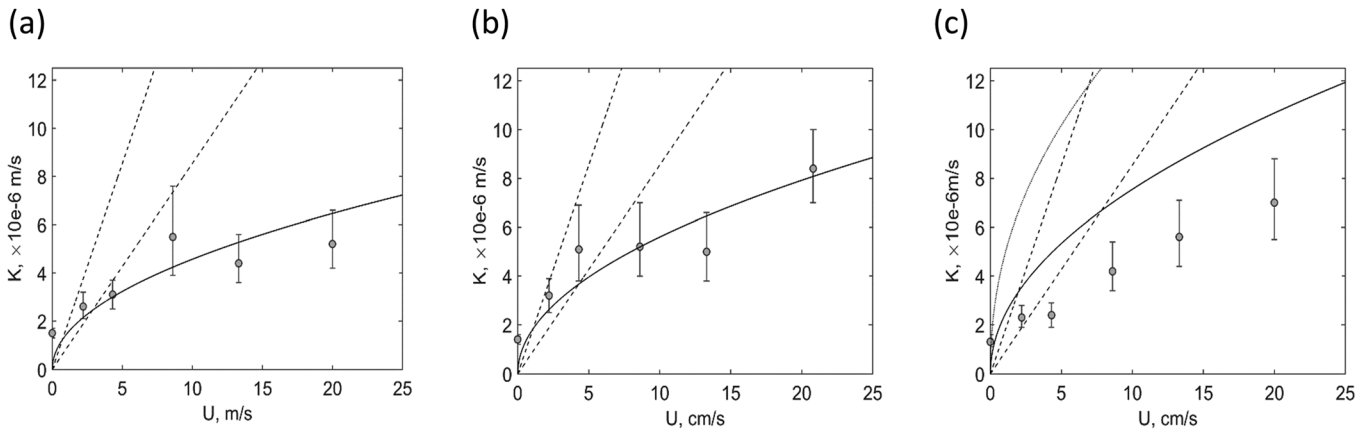

Figure 7. Transfer velocity, K, versus channel velocity, U, for (a) Blade 1, 1 cm×15 cm×100 μm; (b) Blade 2, 1 cm×10 cm×100 μm; (c) Blade 3, 1 cm×5 cm×250 μm. The laminar boundary layer model (equation (7)) is shown with a solid black curve in each plot. The turbulent boundary layer model (equation (6)) is shown by dashed lines. For the upper dashed line, $\delta_V = \frac{10\nu}{u_*}$, and for the lower dashed line, $\delta_V = \frac{5\nu}{u_*}$. The grey curve in Figure 7c denotes the prediction using $K=ED_wD^{-1}Re_D^mSc^{1/3}$ for flow past a circular cylinder. (equation (7.55b) in Incropera and DeWitt (p. 369)

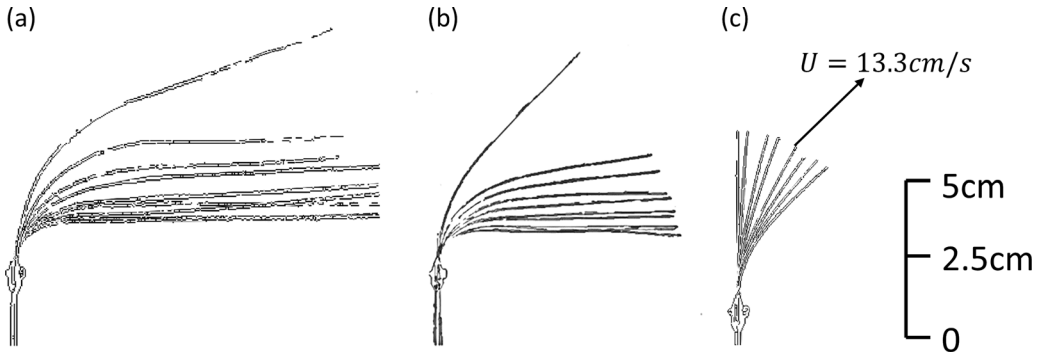

Figure 8. Images of blade posture at U = 2.2, 4.3, 6.5, 8.6, 10.8, 13.3, 15.6, 17.8, and 20.8 cm/s starting from the blade image at the top left and moving to the blade image at the bottom right, respectively. (a) Blade 1, 1 cm×15 cm×100 μm, Ca = 59–5300; (b) Blade 2, 1 cm×10 cm×100 μm, Ca = 17–1600; (c) Blade 3, 1 cm×5 cm×250 μm, Ca = 0.14 to 12. In Figure 8a, the postures at U = 17.8 cm/s and 20.8 cm/s overlap one another. In Figure 8c, the posture at U = 4.3 cm/s and 6.5 cm/s overlap.

values. Specifically, a linear relationship between transfer velocity and current speed was not observed for any of the blades, and the turbulent boundary layer model consistently over-predicted the transfer velocity. Second, for Blade 3, which was nearly vertical (Figure 8), we considered the possible analogy to flow past a circular cylinder, for which the theoretical transfer velocity is $K = ED_w D^{-1} Re_D^m Sc^{1/3}$, with cylinder diameter D replaced by blade width ($D = b$), and empirical coefficients E = 0.683 and m = 0.46, as reported in *Incropera and DeWitt* [1996, p. 369]. In our experiment, $Re_D = \frac{UD}{\nu}$ ranges from 220 to 2080, which falls into the Reynolds number range Re_D = 40 to 4000 in Table 7.2 in *Incropera and DeWitt* [1996, p. 370]. However, this prediction, shown by the grey curve in Figure 7c, also overestimated the measured transfer velocity. The reduced mass flux observed for the nearly vertical blades might be caused by a reduction in relative velocity. Flow stagnates on the front surface of a vertical blade, so that the relative velocity between the water and the blade surface is lower than the condition with flow parallel to the blade surface.

Next, we consider the flux at the meadow scale. To describe the uptake by a meadow based on the bulk concentration in the water outside the meadow, one must consider a two-step flux model, which includes the mass flux across the meadow interface as well as the mass flux at the blade surface [*Lowe et al.*, 2005; *Nepf*, 2011]. For simplicity, we consider an infinite submerged meadow, for which flux into the meadow from the surrounding open water occurs only through the vertical turbulent transport at the top of the canopy (Figure 11). Consider a portion of the meadow with bed area $A = \Delta x \Delta y$. The total two-sided blade area within bed area A is $A_b = 2ah_c \Delta x \Delta y$. Here a is the meadow frontal area per volume, and h_c is the canopy height. The mass flux across the interface at the top of the meadow ($\dot{m}_h$) is

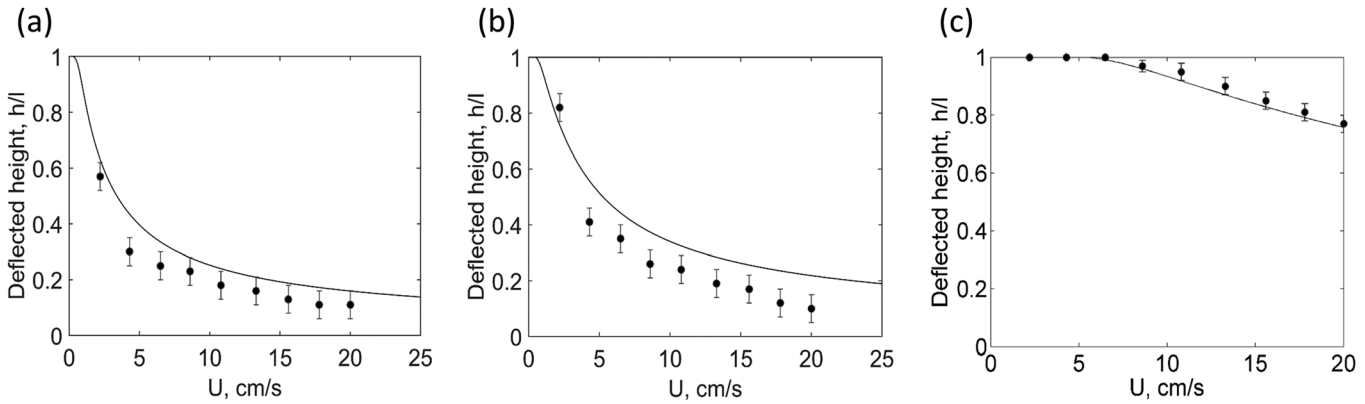

Figure 9. Deflected height normalized by blade length versus channel velocity for (a) Blade 1, 1 cm×15 cm×100 μm, Ca = 59–5300; (b) Blade 2, 1 cm×10 cm×100μm, Ca = 17–1600; (c) Blade 3, 1 cm×5 cm×250 μm, Ca = 0.14–12. The measurements are shown with dots. The solid curve is the predicted by *Luhar and Nepf* [2013, equation (4)]. The uncertainty in measured deflected height was due to the fluctuations in the blade posture. The deflected height, h, was measured vertically from the top of the wooden cylinder to maximum height of the blade, and l denotes the blade length.

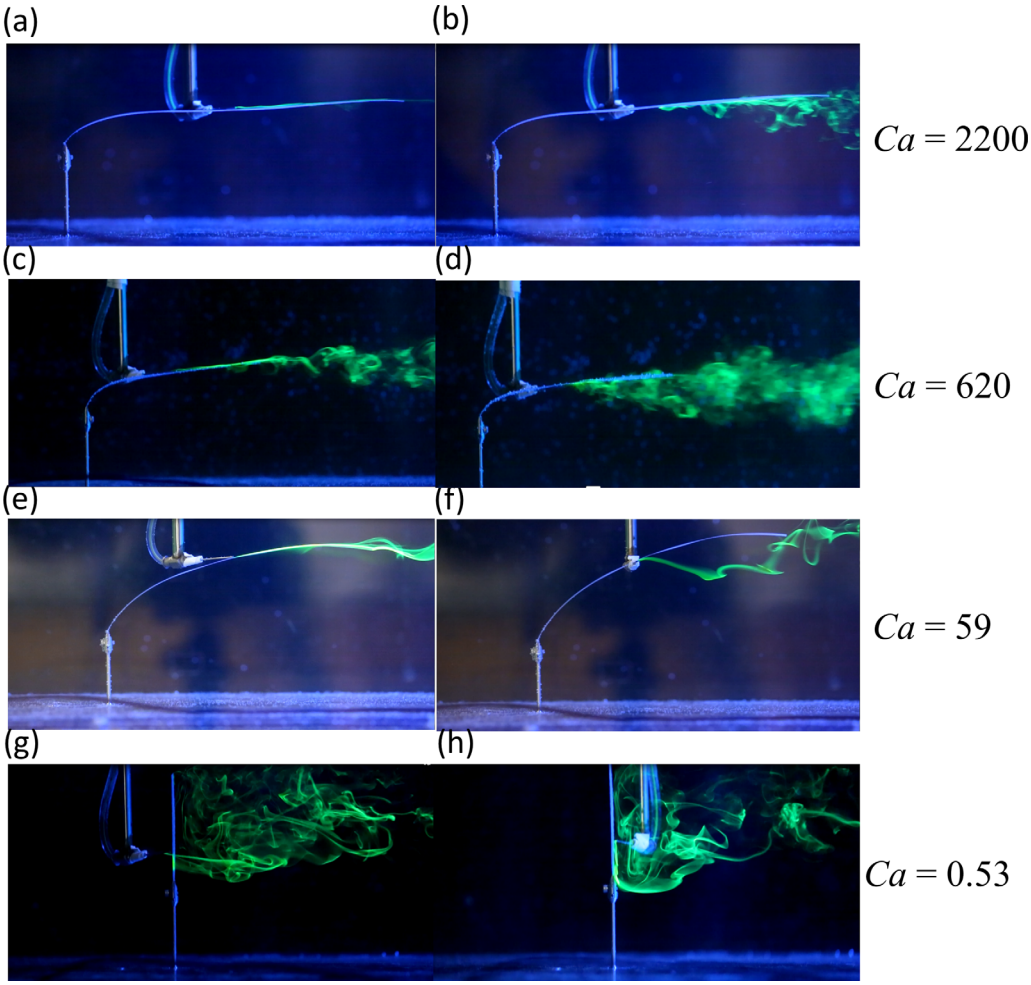

Figure 10. Images extracted from dye test videos for all three blades at different postures. In the (a, c, e, g) left-hand column the dye was injected on the top/front surface; while (b, d, f, h) in the right-hand column, the dye was injected on the bottom/back surface. (a and b) Blade 1, 1 cm×15 cm×100 μm, $U = 13.3$ cm/s and $Ca = 2200$; (c and d) Blade 2, 1 cm×10 cm×100 μm, $U = 13.3$ cm/s and $Ca = 620$; (e) and (f) Blade 1, 1 cm×15 cm×100 μm, $U = 2.2$ cm/s and $Ca = 59$; (g and h) Blade 3, 1 cm×5 cm×250 μm, $U = 4.3$ cm/s and $Ca = 0.53$.

$$\dot{m}_h = K_h \Delta x \Delta y (C_0 - C_c) \tag{15}$$

in which K_h is the transfer velocity between the overflow and the canopy, C_0 is the concentration of the chemical in the overflow, C_c is the concentration inside the canopy. The cumulative mass flux occurring over all blade surfaces within A is

$$\dot{m}_b = K A_b C_c \tag{16}$$

in which K is the transfer velocity at the blade surface, and we have assumed that $C = 0$ at the blade surface, similar to *Bilger and Atkinson* [1992] and *Atkinson and Bilger* [1992]. Specifically, we only consider mass-transfer limited conditions for which the biological uptake keeps up with the physical rate of mass transfer to the surface. At steady state, $\dot{m}_h = \dot{m}_b$, which gives the expression for the net flux $\dot{m}$

$$\dot{m} = \dot{m}_h = \dot{m}_b = \Delta x \Delta y \left(\frac{2Kah_c}{\frac{2Kah_c}{K_h} + 1} \right) C_0 \tag{17}$$

When $2Kah_c \ll K_h$, $\dot{m} = 2Kah_c \Delta x \Delta y C_0$, indicating that the transfer velocity at the blade surface, K, controls the net flux to the meadow; however, when $2Kah_c \gg K_h$, $\dot{m} = K_h \Delta x \Delta y C_0$, indicating that the transfer velocity between the overflow and the meadow controls the net flux to the canopy. Below, we use existing studies to compare $2Kah_c$ and K_h for nutrient flux in seagrass meadows.

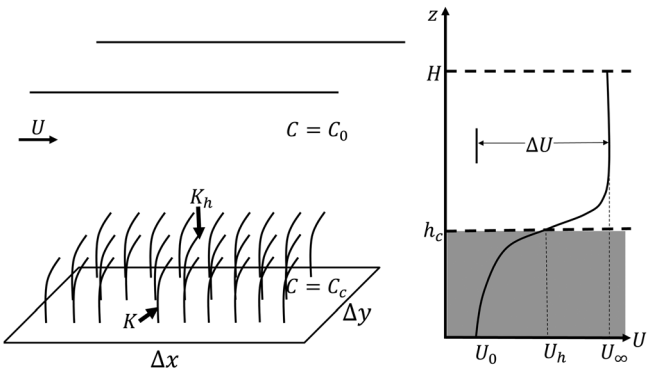

Figure 11. Schematics of the two-step flux model and corresponding velocity profile. Here U is the flow velocity, Δx is the length of the canopy section, Δy is the width of the canopy section, h_c is the canopy height, C_0 is the concentration in the overflow, C_c is the concentration in the canopy, K_h is the transfer velocity between the overflow and the canopy, K is the transfer velocity at the blade surface, U_0 is the velocity in the lower canopy, U_h is the velocity at the top of the meadow, U_∞ is the velocity above the meadow and $\Delta U = U_\infty - U_0$.

First, from *Ghisalberti and Nepf* [2005], $K_h = \frac{\Delta U}{40}$, in which ΔU is the velocity difference between the meadow and the overflow above the meadow. Using velocity profiles measured in real seagrass meadows [*Lacy and Echeverria*, 2011; *Weitzman et al.*, 2013] and in a dynamically-scale meadow model [*Ghisalberti and Nepf*, 2006], the ratio between ΔU and the flow velocity at the top of the meadow (U_h) is $\frac{\Delta U}{U_h} = 1.1$ to 1.8. For coastal currents, a typical depth-averaged velocity might be $U = 0.1$ *to* 0.5 m/s [e.g., *Nepf*, 2011]. Assuming U_h has the same order of magnitude of U, $K_h = O(10^{-2}$ to $10^{-3})$ m/s. Second, for nutrient flux ($D_w \approx 2 \times 10^{-9}$, $Sc = 500$) the laminar boundary layer model gives $\bar{K} = 0.664 D_W \sqrt{\frac{U_h}{\nu L}} Sc^{1/3} = O(10^{-5})$ m/s, using a blade length range of $L = 0.2$ to 0.6 m. Note that U_h overestimates the mean velocity within the canopy, such that $\bar{K}$ is an overestimate. Finally, for typically seagrass meadows, the order of magnitude of ah_c is between $O(10^{-1})$ and $O(10)$. For *Posidonia oceanica*, field measurements by *Infantes et al.* [2012] report the leaf surface area per plant $A_v = 211 \pm 23$ cm^2 and the shoot density $N = 615 \pm 34$ m^{-2}, so $ah_c = NA_v = 13 \pm 2$; for *Zostera marina*, $ah_c = 0.4$ to 2 ([*Moore*, 2004, Figure 4; *McKone*, 2009, Table 2.1]); for *Thalassia testudinum*, field measurements by *Weitzman et al.* [2013, p. 71] give $ah_c = 5 \pm 2$. Even with $\bar{K}$ slightly overestimated we find, $2\bar{K}ah_c = O(10^{-4}$ to $10^{-6})$ ms$^{-1} \ll K_h = O(10^{-2}$ to $10^{-3})$ ms^{-1}. This suggest that under most field conditions the nutrient uptake by a meadow is controlled by the flux at the blade surfaces, i.e., equation (17) reduces to $\dot{m} = \Delta x \Delta y (2Kah_c) C_0$, which in turn suggests that meadow-scale uptake should vary with $U^{0.5}$, following the dependence of K. This result is consistent with field measurements of uptake at the meadow scale. Specifically, under unidirectional current, both *Thomas et al.* [2000] and *Weitzman et al.* [2013] observed uptake rates to a seagrass meadow proportional to $U^{0.4 \pm 0.2}$, consistent with uptake controlled at the blade scale by a laminar boundary layer. One might expect that the highly turbulent conditions found in the field, and in particular the strong turbulence generated at the top of the meadow [e.g., *Ghisalberti and Nepf*, 2002], might trigger a transition from laminar to turbulent boundary layers (e.g., as discussed in *Kosorygin and Polyakov* [1990]). However, the observation that $K \sim U^{0.4 \pm 0.2}$ suggests that the boundary layers remain laminar.

Thomas et al. [2000] measured the uptake rate of ammonium ($D_w = 2 \times 10^{-9}$) by *Thalassia testudinum*. They recorded the transfer rate per bed area (S), which can be converted to transfer velocity per blade area (K) assuming that the average blade length was 0.19 m and the average blade width was 0.9 cm (given in *Weitzman et al.* [2013] for the same species), and using the mean density of 10,200 blade/m^2, given in *Thomas et al.* [2000]. With this conversion, the measured transfer velocity (K) is smaller than the laminar boundary layer prediction, shown by the solid line in Figure 12. However, equation (7) can be fit to the data with a scale factor $\gamma = 0.45$. This fit is shown with a dashed line in Figure 12. Two effects might explain this scale factor. First, within a meadow the individual blades may overlap, sheltering some blade area from flow, which would locally reduce the flux and appear as a reduced transfer velocity. Second, the velocity reported by Thomas was measured at middepth, which would be higher than the velocity within the meadow, which is diminished due to the drag provided by the meadow. Thus, the scale factor fitted above in part reflects an overestimation of in-canopy velocity.

The extension of equation (7) to the field depends on the estimate of an appropriate velocity scale. First, as discussed in the previous paragraph, submerged macrophytes usually grow in meadows, which will reduce the flow velocity around the individual blades, relative to the depth-averaged velocity, so that the definition of reference velocity U in equation (7) needs more careful consideration. U should be scaled as the mean velocity within the meadow (see Figure 12). Second, flow is not evenly distributed over the length of a

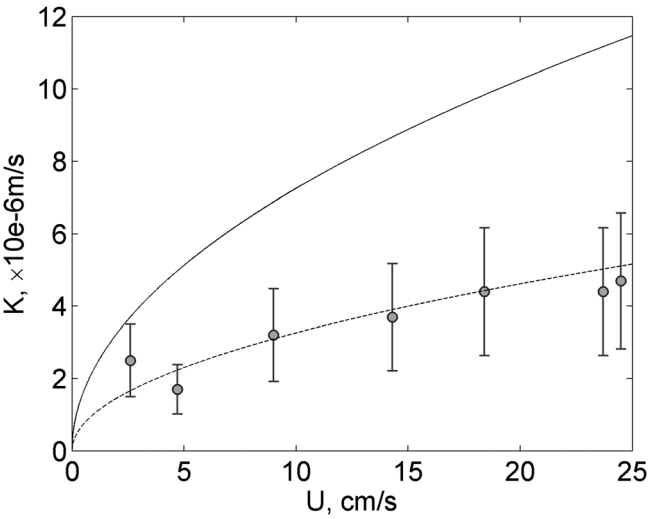

Figure 12. Transfer velocities (K) calculated from the uptake rate per bed area reported for *Thalassia testudinum* in *Thomas et al*. [2000, Table 2]. Conversion to flux per blade area used a typical *Thalassia* blade length of $L = 0.19$ m, a blade width of $b = 0.9$ cm (from *Weitzman et al*. [2013]), and the density 10,200 blade/m^2 reported in *Thomas et al*. [2000]. The laminar boundary layer model (equation (7)) is plotted as a solid line. The dashed curve is the laminar boundary layer model adjusted by a fitting constant, γ, with γ=0.45 producing the best fit.

meadow, such that the location of a blade within the meadow can affect the flux. Specifically, blades near the leading edge of the meadow are exposed to higher velocity, and this condition persists over an adjustment length scale proportional to the meadow density and height [*Chen et al*., 2013]. Consistent with this, *Morris et al*. [2008, Figure 6] observed 20% higher uptake rates at the leading edge of a *Cymodocea nodosa* canopy. Third, for oscillatory flow (waves) the in-canopy velocity attenuation is weaker than for unidirectional flows, such that a higher in-canopy velocity occurs for oscillatory flows, compared to a unidirectional flow with the same depth-averaged current magnitude [*Lowe et al*., 2005; *Luhar et al*., 2010]. Higher in-canopy velocity would enhance canopy-scale mass transfer rates for oscillatory flows, relative to unidirectional flow of the same magnitude. This has indeed been observed for both rigid canopies [*Lowe et al*., 2005] and for seagrass meadows [*Weitzman et al*., 2013]. It is interesting to note that for purely oscillatory flows with wave velocity U_W *Weitzman et al*. [2013] measured $K \propto U_w^{0.5\pm0.2}$, suggesting that a laminar boundary layer model might apply to wave conditions.

The model blades used in this study were smooth. However, in the field seagrass blades are often colonized by epiphytes, which may alter the boundary layer. The impact of roughness on boundary layer flow is described in terms of the roughness Reynolds number, $Re_R = \frac{u_* e}{\nu}$, with e the roughness height. A laminar boundary layer is maintained for $Re_R < 5$ and transition to a fully turbulent boundary layer occurs at $Re_R > 100$ (Figure 11) [*Nikuradse*, 1950]. *Koch* [1994] measured epiphytic cover on real seagrass blades and showed that in many cases, in particular for younger blades, a laminar boundary layer could be maintained even with epiphytic cover, such that equation (7) would apply. For $Re_R < 5$, the epiphytes reside within a laminar boundary layer, so that their uptake, if mass-transfer limited, should also follow a $U^{0.5}$ dependence. For older blades, with larger epiphytes, *Koch* [1994] showed that the boundary layer might be fully turbulent, such that (equation (6)) would apply, leading to a linear dependence on U. For $5 < Re_R < 100$, the boundary layer is in transition, i.e., intermittently laminar and turbulent, such that we might expect mass-transfer limited uptake to follow U^m with m between 0.5 and 1. *Cornelisen and Thomas* [2006] measured the uptake of ammonium and nitrate to epiphytes of size < 35 μm living on *Thalassi testudinum*. Even for the maximum velocity in the study (20 cm/s), 35 μm epiphytes produce $Re_R \approx 1 < 5$, suggesting that these epiphytes resided within a laminar boundary layer. Consistent with this, the uptake rates measured for ammonium and nitrate increased as U^m, with m = (0.41 to 0.85) and (0.51 to 0.57), respectively (95% CI in Table 2 [*Cornelisen and Thomas*, 2006]). The observed velocity dependence is consistent with mass-transfer limited conditions controlled by a laminar boundary layer ($m = 0.5$).

5. Conclusions

Flow over sufficiently pronated, hydraulically-smooth blades resembles flow over a hydraulically-smooth flat plate, for which a laminar boundary layer develops, producing mass-flux that can be represented by a transfer velocity K that increases in proportion to the square root of the current speed ($U^{0.5}$). The laminar boundary layer model, which held when the Cauchy number satisfied $Ca > \approx 60$, predicted K to model blades within uncertainty without any fitting parameters. However, for $Ca < 60$, the blades remained nearly upright and the laminar boundary layer model overestimated the measured K. In the field, epiphytes

produce physical roughness on real seagrass blades, however, for some flow and epiphyte conditions, the boundary layer may remain laminar. In these cases, if the uptake is mass-transfer limited, the uptake to both the blade and to the epiphytes should have dependence on $U^{0.5}$, which is consistent with available field measurements. Finally, a two-layer flux model evaluated for meadow conditions suggests that the uptake at the meadow scale is controlled by the flux at the blade-scale, which would imply that uptake at the meadow scale also increases as $U^{0.5}$, which is consistent with the results of multiple field experiments.

Acknowledgments
This material is based upon work supported by the National Science Foundation under grant EAR 1140970. Any opinions, findings, and conclusions or recommendations expressed in this material are those of the author(s) and do not necessarily reflect the views of the National Science Foundation. The authors thank John MacFarlane for assistance with the chemical flux measurements. All data are provided in the tables and figures, or properly cited and referred to in the reference list. Any additional data may be obtained from Jiarui Lei (email: garylei@mit.edu).

References

Abdelrhman, M. A. (2007), Modeling coupling between eelgrass Zostera marina and water flow, *Mar. Ecol. Prog. Ser.*, *338*, 81–96, doi: 10.3354/meps338081.

Adams, R. G., R. Lohmann, L. A. Fernandez, J. K. MacFarlane, and P. M. Gschwend (2007), Polyethylene devices: Passive samplers for measuring dissolved hydrophobic organic compounds in aquatic environments, *Environ. Sci. Technol.*, *41*(4), 1317–1323, doi:10.1021/es0621593.

Atkinson, M. J., and R. W. Bilger (1992), Effects of water velocity on phosphate uptake in coral reef-flat communities, *Limnol. Oceanogr.*, *37*(2), 273–279.

Barko, J. W., and W. F. James (1998), Effects of submerged aquatic macrophytes on nutrient dynamics, sedimentation and resuspension, in *The Structuring Role of Submerged Macrophytes in Lakes*, edited by E. Jeppesen, et al., pp. 197–214, Springer, N. Y.

Bilger, R. W., and M. J. Atkinson (1992), Anomalous mass transfer of phosphate on coral reef flats, *Limnol. Oceanogr.*, *37*(2), 261–272, doi: 10.4319/lo.1992.37.2.0261.

Boudreau, B. P., and B. B. Jorgensen (Eds.) (2001), The benthic boundary layer: Transport processes and biogeochemistry, Oxford University Press.

Bradley, K., and C. Houser (2009), Relative velocity of seagrass blades: Implication for wave attenuation in low-energy environments, *J. Geophys. Res.*, *114*, F01004, doi:10.1029/2007JF000951.

Chen, Z., C. Jiang, and H. Nepf (2013), Flow adjustment at the leading edge of a submerged aquatic canopy, *Water Resour. Res.*, *49*, 5537–5551, doi:10.1002/wrcr.20403.

Cornelisen, C., and F. Thomas (2006), Water flow enhances ammonium and nitrate uptake in a seagrass community, *Mar. Ecol. Prog. Ser.*, *312*, 1–13, doi:10.3354/meps312001.

Costanza, R., et al. (1997), The value of the world's ecosystem services and natural capital, *Nature*, *387*, 253–260.

Folkard, A. M. (2005), Hydrodynamics of model Posidonia oceania patches in shallow water, *Limnol. Oceanogr. Methods*, *50*(5), 1592.

Fonseca, M. S., M. A. R. Koehl, and B. S. Kopp (2007), Biomechanical factors contributing to self-organization in seagrass landscapes, *J. Exp. Mar. Biol. Ecol.*, *340*(2), 227–246, doi:10.1016/j.jembe.2006.09.015.

Fourqurean, J. W., et al. (2012), Seagrass ecosystems as a globally significant carbon stock, *Nat. Geosci.*, *5*(7), 505–509, doi:10.1038/ngeo1477.

Ghisalberti, M., and H. Nepf (2005), Mass transport in vegetated shear flows, *Environ. Fluid Mech.*, *5*(6), 527–551.

Ghisalberti, M., and H. Nepf (2006), The structure of the shear layer in flows over rigid and flexible canopies, *Environ. Fluid Mech.*, *6*(3), 277–301.

Ghisalberti, M., and H. M. Nepf (2002), Mixing layers and coherent structures in vegetated aquatic flows, *J. Geophys. Res.*, *107*(C2), 3011, doi: 10.1029/2001JC000871.

Grace, J., F. E. Fasehun, and M. Dixon (1980), Boundary layer conductance of the leaves of some tropical timber trees, *Plant Cell Environ.*, *3*(6), 443–450, doi:10.1111/1365-3040.ep11586917.

Greiner, J. T., K. J. McGlathery, J. Gunnell, and B. A. McKee (2013), Seagrass restoration enhances blue carbon sequestration in coastal waters, *PLoS One*, *8*(8), e72469, doi:10.1371/journal.pone.007249.

Hansen, A. T., M. Hondzo, and C. L. Hurd (2011), Photosynthetic oxygen flux by Macrocystis pyrifera: A mass transfer model with experimental validation, *Mar. Ecol. Prog. Ser.*, *434*, 45–55, doi:10.3354/meps09196.

Hurd, C. L., P. J. Harrison, and L. D. Druehl (1996), Effect of seawater velocity on inorganic nitrogen uptake by morphologically distinct forms of Macrocystis integrifolia from wave-sheltered and exposed sites, *Mar. Biol.*, *126*(2), 205–214, doi:10.1007/BF00347445.

Incropera, F. P., and D. P. DeWitt (1996), *Fundamentals of Heat and Mass Transfer*, 4th ed., John Wiley & Sons, Inc., Hoboken, N. J.

Infantes, E., A. Orfila, J. Terrados, M. Luhar, G. Simarro and H. Nepf (2012), Effect of a seagrass (Posidonia oceanica) meadow on wave propagation, *Mar. Ecol. Prog. Ser.*, *456*, 63–72, doi:10.3354/meps09754.

Koch, E. W. (1994), Hydrodynamics, diffusion-boundary layers and photosynthesis of the seagrasses Thalassia testudinum and Cymodocea nodosa, *Mar. Biol.*, *118*(4), 767–776, doi:10.1007/BF00347527.

Koch, E. W., et al. (2009), Non-linearity in ecosystem services: Temporal and spatial variability in coastal protection, *Frontiers Ecol. Environ.*, *7*(1), 29–37, doi:10.1890/080126.

Kosorygin, V., and N. Polyakov (1990), Laminar boundary layers in turbulent flows, in *Laminar-Turbulent Transition*, edited by D. Arnal and R. Michel, 573–578, Springer, Novosibirsk, USSR, doi:10.1007/978-3-642-84103-3.

Kundu, P., and I. Cohen (2002), *Fluid Mechanics*, 2nd ed., Academic Press, San Diego, Calif.

Lacy, J. R., and S. Wyllie-Echeverria (2011), The influence of current speed and vegetation density on flow structure in two macrotidal eelgrass canopies, *Limnol. Oceanogr. Fluid Environ.*, *1*(1), 38–55.

Lohmann, R. (2012), Critical review of low-density polyethylene's partitioning and diffusion coefficients for trace organic contaminants and implications for its use as a passive sampler, *Environ. Sci. Technol.*, *46*(2), 606–618.

Lowe, R. J., J. R. Koseff, S. G. Monismith, and J.L. Falter (2005), Oscillatory flow through submerged canopies: 2. Canopy mass transfer, *J. Geophys. Res.*, *110*, C10017, doi:10.1029/2004JC002789.

Luhar M., S. Coutu, E. Infantes, S. Fox, and H. Nepf (2010), Wave induced velocities inside a model seagrass bed, *J. Geophys. Res. Oceans*, *115*(C12).

Luhar M., and H. Nepf (2011), Flow-induced reconfiguration of buoyant and flexible aquatic vegetation, *Limnol. Oceanogr. Methods*, *56*(6), 2003–2017, doi:10.4319/lo.2011.56.6.2003.

Luhar, M., and H. Nepf (2013), From the blade scale to the reach scale: A characterization of aquatic vegetative drag, *Adv. Water Resour.*, *51*, 305–316, doi:10.1016/j.advwatres.2012.02.002.

McKone, K. (2009), Light available to the seagrass Zostera marina when exposed to currents and waves, PhD thesis, Univ., College Park, Md.

Moore, K. A. (2004), Influence of seagrasses on water quality in shallow regions of the lower Chesapeake Bay, *J. Coastal Res.*, *20*, 162–178, doi:10.2112/SI45-162.1.

Morris, E. P. and G. Peralta, F. G. Brun, L. van Duren, T. J. Bouma, J. L. Perez-Llorens (2008), Interaction between hydrodynamics and seagrass canopy structure: Spatially explicit effects on ammonium uptake rates, *Limnol. Oceanogr. Methods*, *53*(4), 1531–1539, doi:10.4319/lo.2008.53.4.1531.

Nepf, H. M. (2011), Flow over and through biota, Treatise on estuarine and coastal science, in edited by E. Wolanski and D. McLusky, 267–288, Elsevier, San Diego, Calif.

New Jersey Department of Environmental Protection (NJDEP), (2010), Site remediation program, Guidance Documents, Remediation Standards, Chemical properties table.

Nikuradse, J. (1950), *Laws of flow in rough pipes*, National Advisory Committee for Aeronautics, Wash.

Nishihara, G. N., and J. D. Ackerman (2006), The effect of hydrodynamics on the mass transfer of dissolved inorganic carbon to the freshwater macrophyte Vallisneria Americana, *Limnol. Oceanogr. Methods*, *51*(6), 2734–2745, doi:10.4319/lo.2006.51.6.2734.

Nishihara, G. N., and J. D. Ackerman (2009), Diffusive boundary layers do not limit the photosynthesis of the aquatic macrophyte Vallisneria Americana at moderate flows and saturating light levels, *Limnol. Oceanogr. Methods*, *54*(6), 1874–1882, doi:10.4319/lo.2009.54.6.1874.

Romero, J., Lee, K. S., Pérez, M., Mateo, M. A., and T. Alcoverro (2006), Nutrient dynamics in seagrass ecosystems, in *Seagrasses: Biology, Ecology and Conservation*, edited by A. W. D. Larkum, R. J. Orth, and C. M. Duarte, 227–254, Springer, Dordrecht, doi:10.1007/1-4020-2983-7_9.

Rominger, J. T. (2014), Hydrodynamic and transport phenomena at the interface between flow and aquatic vegetation: From the forest to the blade scale, Doctoral dissertation, MIT, Cambridge, Mass.

Stevens, C. L., and C. L. Hurd (1997), Boundary-layers around bladed aquatic macrophytes, *Hydrobiologia*, *346*(1-3), 119–128.

Taylor, J. (1997), *An Introduction to Error Analysis: The Study of Uncertainties in Physical Measurements*, 2nd ed., University Science Books, N. Y.

Thomas, F. I. M., C. D. Cornelisen, and J. M. Zande (2000), Effect of water velocity and canopy morphology on ammonium uptake by seagrass communities, *Ecology*, *81*(10), 2704–2713, doi:10.1890/0012-9658(2000)081%5B2704:EOWVAC%5D2.0.CO;2.

Touchette, B. W., and J. M. Burkholder (2000), Review of nitrogen and phosphorus metabolism in seagrasses, *J. Exp. Mar. Biol. Ecol.*, *250*(1), 133–167, doi:10.1016/S0022-0981(00)00195-7.

Waycott, M., B. J. Longstaff, and J. Mellors (2005), Seagrass population dynamics and water quality in the great barrier region: A review and future research directions, *Mar. Pollut. Bull.*, *51*(1), 343–350, doi:10.1016/j.marpolbul.2005.01.017.

Weitzman, J. S., K. Aveni-Deforge, J. R. Koseff, and F. Thomas (2013), Uptake of dissolved inorganic nitrogen by shallow seagrass communities exposed to wave-driven unsteady flow, *Mar. Ecol. Prog. Ser.*, *475*, 65, doi:10.3354/meps09965.

White, F. M. (2008), Fluid Mechanics, Sixth ed., McGraw-Hill, Boston, Mass.